arXiv:astro-ph/9811248v1 16 Nov 1998

Accuracy of Mesh Based Cosmological Hydrocodes: Tests and Corrections

Renyue Cen and Jeremiah P. Ostriker

Princeton University Observatory, Princeton, NJ 08544

(cen,jpo)@astro.princeton.edu

Received _____; accepted _____

ABSTRACT

We perform a variety of tests to determine the numerical resolution of the cosmological TVD eulerian code developed by Ryu et al. (1993). Tests include 512^3 and 256^3 simulations of a $P_k \propto k^{-1}$ spectrum to check for self-similarity and comparison of results with those from higher resolution SPH and grid-based calculations (Frenk et al. 1998). We conclude that in regions where density gradients are not produced by shocks the code degrades resolution with a Gaussian smoothing (radius) length of 1.7 cells. At shock caused gradients (for which the code was designed) the smoothing length is 1.1 cells. Finally, for β model fit clusters, we can approximately correct numerical resolution by the transformation $R_{core}^2 \rightarrow R_{core}^2 - (C\Delta l)^2$, where Δl is the cell size and $C = 1.1 - 1.7$. When we use these corrections on our previously published computations for the SCDM and ΛCDM models we find luminosity weighted, zero redshift, X-ray cluster core radii of $(210 \pm 86, 280 \pm 67)h^{-1}$kpc, respectively, which are marginally consistent with observed (Jones & Forman 1992) values of $50 - 200h^{-1}$kpc. Using the corrected core radii, the COBE normalized SCDM model predicts the number of bright $L_x > 10^{43}$erg/s clusters too high by a factor of ~ 20 and the ΛCDM model is consistent with observations.

Subject headings: Cosmology: large-scale structure of Universe – hydrodynamics – numerical method

1. Introduction

Two types of hydrodynamic codes are currently in use for cosmological applications: mesh based codes pioneered by Vishniac and co-workers (Chiang, Ryu, & Vishniac 1989; Ryu, Vishniac, & Chiang 1990) and Cen and co-workers (Cen et al. 1990; Cen 1992) and used by several groups including a TVD ("Total Vaviation Diminishing") variant (Ryu et al. 1993) or a PPM ("Piecewise Parabolic Method") variant (Bryan et al. 1995), and, alternatively, particle based smooth particle hydrodynamics codes ("SPH") used by a variety of groups (Evrard 1988; Hernquist & Katz 1989; Steinmetz 1996; Owen et al. 1998a). The latter codes can concentrate computational resources into the highest density regions of greatest interest, but they suffer in low density regions, at caustics, and, due to the large computational overhead, they have relatively small particle number and hence have relatively poor mass resolution which can induce two body relaxation even in the high density regions (Kuhlman, Melott, & Shandarin 1996; Steinmetz & White 1997).

But the mesh codes also have, along with their virtues of accurate treatment of shocks and caustics, good mass resolution, known accuracy and convergence properties etc, quite serious weaknesses, the primary among them being poor spatial resolution in the high density regions. A detailed comparison of five codes – three independent mesh codes and two independent SPH codes comparing the virtues and details of the two approaches was presented in Kang et al. (1994b). Another major such comparative project was completed recently (Frenk et al. 1998) with a still wider range of codes being tested.

What is the accuracy of a mesh code in resolving structures comparable to or smaller than the mesh size? A quantitative assessment of this in the cosmological context was presented by Cen (1992) for an aerodynamics-based cosmological hydrodynamic code, which has an effective artificial viscosity of known properties. Anninos & Norman (1996) did some very interesting convergence tests on X-ray clusters by varying numerical resolution using

a multi-grid eulerian hydrocode. Bryan & Norman (1998) examined resolution effect on various quantities related to simulated X-ray clusters using PPM eulerian code (Bryan et al. 1995). Owen et al. (1998b) have studied various scaling properties in scale-free ($P_k \propto k^{-1}$), adiabatic SPH simulations. In the present paper we examine the TVD shock capturing code originally developed by Harten (1984) and reformulated with gravity for high mach number, cosmological applications by Ryu et al. (1993). This code has been used by Cen, Ostriker and co-workers to study the properties of X-ray clusters of galaxies and Lyman alpha clouds, and is being used for work on galaxy formation. The primary result, which we find, can be stated simply. In general, the code smooths structure with a gaussian filter $e^{-r^2/2\sigma_r^2}$ such that $\sigma_r = \alpha\Delta l$ where Δl is the cell size and α is the number which we are interested in fixing through empirical experiments. Smoothing separately in the three directions, $\sigma_r^2 = \sigma_x^2 + \sigma_y^2 + \sigma_z^2$. Alternatively phrased, an object of true gaussian radius r_{true} will have computed radius r_{comp}

$$r_{comp}^2 = r_{true}^2 + r_{res}^2 \tag{1}$$

where

$$r_{res} = 1.18\sigma_r; \qquad \sigma_r \equiv \alpha\Delta l \tag{2}$$

where the coefficient 1.18 comes from the fact that our fitted radius (i.e., core) is defined at a location where the density drops to half the central value. An important, new finding from the current study is that the TVD shock-capturing code has different resolutions in different regions. We find that the code has a resolution of ~ 1.1 cells (i.e., $\alpha = 0.95$) near shock fronts, while its resolution in non-shocking, high density regions is lower than in the shock fronts, $\alpha = 1.4$. Since the scheme has been optimized for capturing shocks (rather than, for example, contact discontinuities), we should not be surprised by this variation. The paper is organized as follows: §2 describes the computations to derive the empirical resolution of the code, §3 presents an application of the results to previous published simulations using the TVD code and §4 gives conclusions.

2. Computations

An extremely difficult aspect of this problem is to design a test, with a known, analytically computable solution, that is also sufficiently realistic to have a bearing on the problems of astrophysical interest: in this case the properties of X-ray clusters. N. Kaiser and also S. White have pointed out to us that, if the initially assumed spectrum of density perturbations were a power law, with $P_k = Ak^{-1}$ being the most appropriate choice, then for $\Omega_0 = 1$, some strict scaling relations must hold in a perfect simulation. Specifically, if one were to look at a given population, e.g., the most massive 10% of the bound objects in the universe, then (see Kaiser 1986) in an adiabatic calculation, their characteristic sizes should scale as $(1+z)^{-2}$ and their average temperatures scale as $(1+z)^{-1}$. In our recent simulations of various specific models for the growth of structure we did not find that these scaling laws were very well satisfied. Examining Figures (11) and (12) of Kang et al. (1994a; KCOR hereafter) we see that the expected scaling law for the temperature is satisfied to sufficient accuracy (given the observed statistical fluctuations due to the relatively small computed sample of clusters), but the cluster radius evolution is significantly less steep than is expected. There are a variety of potential explanations for these facts. Three of the most plausible ones are as follows.

1. The actual spectrum of the studied CDM model is not fit by $P_k \propto k^{-1}$ with sufficient precision to make self-similarity an expected outcome.

2. Resolution corrections due to numerical inaccuracy are redshift dependent and account for the departure from the expected scaling.

3. The displayed sample was chosen to be of fixed luminosity: $L_x(0.5 < E < 4.5keV) > 10^{43}$erg/s, which is not a sample defined in a scale free way.

To see which, if any, of these explanations is true, and to better enable us to make

appropriate resolution corrections, we computed two new simulations of a power law spectrum $P_k = Ak^{-1}$ of initial density perturbations with (512^3 cells, 256^3 particles) and (256^3 cells, 128^3 particles), respectively. A simulation box of size of $80h^{-1}$Mpc comoving is used in both simulations, giving a cell size and nominal resolution of (156 h^{-1}kpc comoving, 312 h^{-1}kpc comoving), respectively. Other parameters, in the familiar notation, were chosen to be $\sigma_8 = 1$, $h = 0.5$, $\Omega_{CDM} = 0.95$, $\Omega_b = 0.05$ to correspond well to prior work. To ensure that the "truth" remains the same in the two simulations, the initial realizations in the two simulations are exactly the same, with the power spectrum being cut off at the Nyquist frequency of the 256^3 box for both simulations (A smooth but rather sharp filter, $\cos[\pi k/2k_{nyq,256}]^{1/4}$, is applied to the power law spectrum to minimize real space oscillations but maintain the power law slope as closely as we can).

Figure 1 shows the redshift dependence of the temperature (equally weighted) of the absolutely brightest clusters defined in scale-free fashion: the most massive clusters (within a radius of $1.0h^{-1}$Mpc comoving) which contain 20% of total mass in the universe at each epoch. The temperature of each cluster is the X-ray emission-weighted average over the indicated sphere. Note that the selection method of clusters at different redshifts used here is somewhat different from that used in KCOR, which was not scale-free: only the bright clusters with luminosity $L_x(0.5 < E < 4.5keV) > 10^{43}$ erg/s were selected at each redshift. Nevertheless one sees a behavior of the temperature of the set of brightest clusters qualitatively similar to what was shown in KCOR (Figure 13 in KCOR): in both cases the temperature scales with redshift approximately as expected: $T_x = \text{const.}(1+z)^{-1}$.

We plot, in Figure 2, r_{100} versus redshift. Here, r_{100} is the average radius of top 20% (in mass) clusters in each model at each redshift within which the average density of each cluster is $100\bar{\rho}(z)$ [$\bar{\rho}(z)$ is the global mean at z]. As r_{100} is much larger than the cell size at all times shown, resolution effects should be minimal. We see that the agreement between

the simulation and the analytic prediction (Kaiser 1986) is satisfactory.

Now let us turn to the core radii. These are much smaller than r_{100} and may be unresolved in our simulation. Figure 3 shows the redshift dependence of the average cluster core radius for the same set of clusters (top 20% in mass). Each cluster core is found by fitting the simulated cluster emissivity profile to the following equation

$$j = \frac{j_0}{[1 + (r/r_{core})^2]^2} \tag{3}$$

As in KCOR (see Figure 12 there) we see that the cluster core radius does not scale with redshift as predicted analytically. Comparison shows that the departure from the expected scaling is as great for the power law model as for the real CDM-like spectrum, indicating that spectral curvature is not an important factor over the redshift range ($0 < z < 1$) considered. Furthermore, the scaling behaviors are similar when we select the clusters in this powerlaw simulation using the same criterion as in KCOR. Thus, both explanations (1) and (3) are false and it is likely that the problem is due to the redshift dependence of numerical resolution.

Let us now examine the ansatz mentioned in the introduction. We fit the computed core radius r_{comp} (in comoving units) with an equation of the form

$$r_{comp}^2(z) = r_{true}^2(z) + 1.39\alpha^2(z)(\Delta l)^2 \tag{4}$$

The first term on the right hand side represents the true core size for the *actual* model computed and the second term is r_{res}^2, where Δl is the comoving cell size of a simulation. There are two variables to be solved at each epoch. Since the two simulations have identical initial conditions, r_{true} should be the same in the two simulations for clusters selected in the same, scale-free way. This allows us to solve the above equation for $\alpha(z)$ at each redshift and then $r_{true}(z)$, both of which are displayed in Figure 4. Two points are immediately evident. First, the resolution of the simulation is indeed *redshift dependent*, as seen in the

dependence of α on z, ranging from 0.95 ± 0.05 at redshift one to a 1.40 ± 0.05 at redshift zero. Second, the derived "true" core size, r_{true}, at first sight, strongly disagrees with the naive analytical expectation, which states $r_{true} \propto (1+z)^{-\gamma}$ (where γ is a constant thought to be ~ 1.0). Both of these points deserve a thorough understanding.

We address the second point first. First we note that the assumed power law spectrum has no characteristic scale and presumably would give $r_{true} \rightarrow 0$. However, the actual simulation does not possess a perfect k^{-1} power law spectrum. In fact, the actual input power spectrum to the simulation is $k^{-1}\cos(\pi k/2k_{nyq,256})^{1/4}$ for $k \in [0.0785, 10.053]$ h Mpc^{-1} comoving (where the lower limit is due to the limited box size and the upper limit is, $k_{nyq,256}$, the Nyquist frequency for the 256^3 simulation box) and zero otherwise. Figure 5 shows the linear r.m.s. density fluctuations as a function of top-hat comoving radius for the actual smoothed, truncated power law spectrum (solid curve), which is used in the simulations. An ideal, untruncated k^{-1} power law spectrum would have the the fluctuation spectrum as indicated by the dashed line. We see that the truncated power law spectrum introduces a natural turnover scale around $0.2 - 0.3h^{-1}$ Mpc in the density fluctuation spectrum. Therefore, in the actual simulations under consideration, a core can only develop *at a size* $\sim 0.2 - 0.3h^{-1}$ Mpc *or greater.* This explains why the derived true core size shown in Figure 4 is constant (within the small noise) from $z = 1$ to $z = 0$, simply because the true core size for an untruncated power law spectrum at $z \sim 0$ (with the adopted normalization of $\sigma_8 = 1$) either happens to be $\sim 0.25h^{-1}$ Mpc or is still smaller than $\sim 0.20 - 0.30h^{-1}$ Mpc. Thus, at all higher redshifts, the derived "true" core size represents what is introduced due to the truncation of the power, resulting in a nearly constant core size over the redshift range examined here.

As a consequence, a more conservative approach is possible to obtain a bound on our resolution (i.e., on α). If we assume that the true core radius is zero at all redshift, i.e.,

$r_{true} = 0$, then the measured core radius is entirely due to finite numerical resolution (either in the initial conditions or in the subsequent hydrodynamic simulations). We find a redshift dependent bound on the resolution: at $z = 1$, $\alpha < 1.2 - 1.7$ and $z = 0$, $\alpha < 1.5 - 2.0$.

Let us now turn to the first point: is the derived value of α and its redshift dependence reasonable? It is not hard to explain results with regard to this. A shock-capturing code such as the one examined here is designed to resolve shocks. In fact, the code is shown to be able to resolve a shock in about 1-2 cell (top-hat) (Ryu et al. 1993), which is consistent with what is found here in resolving early clusters since at these early times the regions which dominate X-ray emission are just undergoing shocking. On the other hand, the code is also known to be able to resolve contact discontinuities or non-shocking, large density gradients at a lower resolution of 2-3 cells (top-hat) (Ryu et al. 1993). This is again in agreement with the found resolution for clusters at lower redshifts ($\sim 1.0 - 2.0$ cells [Gaussian]), where shocks are far outside of cluster centers and cumulative diffusion with time tends to smooth the high density central cluster regions.

As a final and quite significant check we show, in Figure 6, the result taken from Frenk et al. (1998), where the solid dots are the density profile (spherically averaged) of a cluster in a controlled volume of a CDM universe computed by the same TVD code used here with $N = 512$ cells and nominal resolution (i.e., cell size) of $62.5h^{-1}$kpc. The open circles and solid curve represent a fit to the average profile of all the simulations from Frenk et al. (1998), which is dominated by a few highest resolution simulations in the inner region ($r < 0.1h^{-1}$Mpc). The dashed curve is the smoothed profile of the solid curve by a gaussian with $\sigma_r = 1.65\Delta l$ (i.e., with $\alpha = 1.65$). We see the result computed in the core regions by our code does in fact correspond well to a gaussian smoothed version of the true density profile if the smoothing length is taken to be 1.65 cells. This particular simulated cluster is probably more advanced than any cluster in the current simulations. Therefore, a larger

value of α is entirely to be expected, but is consistent with the bound on α obtained above.

3. Applications

Let us now apply the derived results on core radii to our previous computations of X-ray clusters of galaxies which had a box size of $85h^{-1}$Mpc and a cell size of $315h^{-1}$kpc. From Figure 6b of Kang et al. (1994) for the $\Omega_0 = 1$ SCDM model we have obtained the luminosity-weighted average core radius at each redshift, $r_{core,comp}$. Then, we use equation (1) to compute $r_{core,true}$ at each redshift, given α as shown in Figure 4. Since this SCDM model has comparable amplitudes of the density fluctuations on the relevant scales and comparable abundance of clusters of galaxies compared to the power law model tested here, it seems appropriate to directly use α as shown in Figure 4.

In order to make meaningful assessments we need to have an estimate of error on the derived α. We obtain the error on α by finding individual α for each pair of clusters found in the two different resolution simulations. For clusters selected in a self-similar way as indicated above, we find that 4 out of 4 clusters in the high resolution simulation have the counterparts in the low resolution simulation at $z = 0$, 5 out of 5 at $z = 0.3$, 6 out of 6 at $z = 0.5$, 6 out of 9 at $z = 1.0$, and 12 out of 15 at $z = 2.0$. We do not include clusters that are not paired in the two simulations in computing the errors on α. We find the 1σ statistical error of α to be $(0.15, 0.097, 0.049, 0.048, 0.061)$ at redshift $z = (0.0, 0.3, 0.5, 1.0, 2.0)$, respectively, with the dispersion being $(0.25, 0.19, 0.11, 0.11, 0.20)$. The identification of each pair of clusters is unambiguous with 3-d r.m.s displacement being less than one simulation cell at all epochs examined.

If a cluster's average velocity dispersion with some large radius (a few times the core radius) is fixed and the emissivity profile is assumed to be that as in equation (3),

then one can show that approximately $L_x \propto r_{core}^{-1}$. Further assuming that the luminosity function has a slope of -2, i.e., $n(>L) \propto L^{-2}$, as indicated by both simulations and observations (see Figures 1-4 of Kang et al. 1994), we are able to correct the number of bright X-ray clusters. Figure 7 shows the computed core radii, the corrected core radii, the computed number of X-ray clusters brighter than $L > 10^{43}$ erg/sec, and corrected number of X-ray clusters brighter than $L > 10^{43}$ erg/sec, in the SCDM model, from redshift zero to one. The errorbars on $r_{core,corr}$ and n_{corr} are obtained by propagating errorr through the following equations: $\Delta r_{core,corr}/r_{core,corr} = \Delta\alpha/\alpha$, $L_x \propto r_{core}$ and $n(>L_x) \propto L_x^{-2}$ (see below for a discussion on errors). The most significant result from this exercise is that the apparent positive evolution of bright X-ray clusters previously found in the SCDM model seems due to the fact that the lower redshift clusters are relatively more underresolved. Correcting this redshift-dependent resolution effect seems to show that the bright clusters are consistent with no evolution (or weak evolution) up to redshift one, in better agreement with observations and semi-analytic studies (Henry et al. 1992). Figure 8 shows the same results for the ΛCDM model (Cen & Ostriker 1994). Since the ΛCDM model is significantly different from the power law model computed here, it is somewhat tricky as to how to apply α derived here to the ΛCDM model. We make the following observation. Since a $\sigma_8 \sim 0.5$ power law model has approximately the same cluster abundance as the ΛCDM model (e.g., Cen 1998), it seems most appropriate to apply the α at $z = 1$ in the power law model to clusters at $z = 0$ in the ΛCDM model. For clusters in the ΛCDM model at higher redshift we simply use our best estimates of α by extrapolation. Note that the corrected zero redshift luminosity weighted X-ray core radii in the (SCDM,ΛCDM) models are $(210 \pm 45, 280 \pm 60)h^{-1}$kpc, respectively. This errorbars on r_{true} are estimated based on the errors on r_{comp}. This is to be compared with observations by Jones & Forman (1992) of $50 - 200h^{-1}$kpc.

For both models we see that our previous computations have overestimated the core

radii by factors of $1.7 - 3.1$ and underestimated the number of bright clusters by a varying factor from about 3 to 10. We were aware of the resolution issue when we wrote Kang et al. (1994) and Cen & Ostriker (1994) and thus treated the computed numbers of bright clusters as lower bounds to the true numbers. Thus, the present exercise has the primary effect of strengthening our previous conclusion that the COBE normalized CDM model overpredicts the number of bright X-ray clusters by a very large factor (~ 20). The ΛCDM model, revised to include corrections described here, would be approximately consistent with observations [note that we found a plotting error in our previous published results: the vertical values of the simulated results in Figure 1 of both Kang et al. (1994) and Cen & Ostriker (1994) are too large by a factor of $\ln(10) = 2.3$; our revised statement above with regard to the number of bright clusters in the two models includes the correction of this error].

Finally, let us estimate the systematic errors associated with the corrected luminosity of a cluster using the resolution correction method described here. Assuming that $L_x \propto r_{core}^{-1}$ and taking the form $L_{true} = (D \pm \Delta D) L_{comp}$, we have $D = r_{comp}/r_{true} = \sqrt{1 + 1.18\alpha\Delta l/r_{true}}$. Taking the $z = 0$ solid square in Figure 7 as an example (which has largest extrapolation among our results) with $\alpha = 1.4$ and $r_{true} = 0.65\Delta l$, we have $D = 1.9$; i.e., the correction (due to systematic error) on the X-ray luminosity of clusters at $z = 0$ is as large as the computed value, it thus appears that systematic errors associated with extrapolated X-ray cluster luminosity is still very large for the published simulations. But, we note that, if we trust the derived values of r_{true}, then in new simulations at a dynamic range of 768^3 now achievable with the same box size ($L = 85h^{-1}$Mpc) as the previously published ones, the resolution correction would be small with $D = 1.38$, i.e., 38% correction (systematic error), and relatively reliable. The associated errorbar on D (statistical error) would be $\Delta D/D = \Delta r_{comp}/r_{comp} = \Delta\alpha/\alpha = 0.15/1.4 = 10.7\%$ for the clusters in the SCDM model at $z = 0$. The clusters in the ΛCDM model at $z = 0$, $(D, \Delta D)$ would be $(1.20, 0.05)$. Hence

a 95% percent upper bound (including both systematic and statistical errors) would have an upward correction on computed value of only 1.97 and 1.50, respectively, for clusters at $z = 0$ in the new simulations of SCDM and ΛCDM models. Corrections for clusters at higher redshifts would be still smaller. A larger simulation box would diminish the statistical errorbars, while higher resolution would further reduce systematic errorbars.

4. Conclusions

To summarize our results, we find an effective gaussian smoothing length of approximately 1.7 cells except in regions where the density gradients are caused by shocks (for which the TVD code is optimized) where the smoothing length is approximately 1.1 cells. Density profiles can be deconvolved with the smoothing length when the correction is small: $R^2_{core,true} = R^2_{core,comp} - (C\Delta l)^2$, where $C = 1.1 - 1.7$. But results are not to be trusted if the computed core radii of clusters are less than $1.1\Delta l$.

Applying the derived resolution effect to our previous X-ray cluster simulations we find that our previous computations underestimate the number of bright clusters by a varying factor from about 3 to 10. We estimate that the error on the corrected clusters luminosities are still very large, thus the correction is not reliable. In addition, the redshift evolutions of bright clusters in the models are altered to varying extent. Our previous conclusion that the COBE normalized CDM model overpredicts the number of bright X-ray clusters by a very large factor is greatly strengthened. Finally, we note that, with new simulations at a dynamic range of 768^3 now achievable with the same box size ($L = 85h^{-1}$Mpc) as the previously published ones, the resolution correction would be small [$(38\%, 20\%)$, respectively] and relatively reliable.

We are happy to acknowledge support from grants NAGW-2448, NAG5-2759,

AST91-08103 and ASC93-18185 and useful conversations with L. Hernquist, N. Kaiser, U. Pen and S. White. It is a pleasure to acknowledge Pittsburg Supercomputing Center for allowing us to use Cray C90 supercomputer. We would like to thank the hospitality of ITP during our stay when this work is completed, and the financial support from ITP through the NSF grant PHY94-07194. Some of the computation was performed at the Princeton SGI Origin 2000 which is supported by grant from the NCSA Alliance Center.

REFERENCES

Anninos, P., & Norman, M.L. 1996, ApJ, 459, 12

Bryan, G.L., Cen, R., Norman, M.L., Ostriker, J.P., & Stone, J.M. 1994, ApJ, 428, 405

Bryan, G.L., Norman, M.L., Stone, J.M., Cen, R., & Ostriker, J.P. 1995, Comp. Phys. Comm., 89, 149

Bryan, G.L., & Norman, M.L. 1998, ApJ, 495, 80

Cen, R. 1992, ApJS, 78, 341

Cen, R., Liu, F., Jameson, A., & Ostriker, J.P. 1990, ApJL, 362, L41

Cen, R., & Ostriker, J.P. 1994, ApJ, 429, 4, LCDM

Cen, R. 1998, ApJ, in press

Chiang, W.H., Ryu, D., and Vishniac, E.T. 1989, ApJ, 339, 603

Evrard, A. E. 1988, MNRAS, 235, 911

Frenk, C.S. et al. 1998, in preparation

Henry, J.P., Gioia, I.M., Maccacaro, T., Morris, S.L., Stocke, J.T., & Wolter, A. 1992, ApJ, 386, 408

Hernquist, L. & Katz, N. S. 1989, ApJS, 64, 715

Jones, C., & Forman, W. 1992, in "Clusters and Superclusters of Galaxies", ed. A.C. Fabian (Kluwer, Netherland), p49

Kang, H., Cen, R., Ostriker, J.P., & Ryu, D. 1994a, ApJ, 428, 1 (KCOR)

Kang, H., Ostriker, J.P., Cen, R., Ryu, D., Hernquist, L., Evrard, A.E., Bryan, G.L., & Norman, M.L. 1994b, ApJ, 430, 83

Kuhlman, B, Melott, A.L., & Shandarin, S. 1996, ApJ, 470, L41

Owen, J.M., Villumsen, J.V., Sharpiro, P.R., & Martel, H. 1998a, ApJS, 116, 155

Owen, J.M., Weinberg, D.H., Evrard, E., Hernquist, L., & Katz, N. 1998b, ApJ, 503, 160

Ryu, D., Vishniac, E.T., and Chiang, W.H. 1990, ApJ, 354, 389

Ryu, D., Ostriker, J.P., Kang, H., & Cen, R.Y. 1993, ApJ, 414, 1

Steinmetz, M. 1996, MNRAS, 278, 1005

Steinmetz, M., & White, S.D.M. 1997, MNRAS, 288, 545

This manuscript was prepared with the AAS LaTeX macros v4.0.

Fig. 1.— shows the redshift dependence of the temperature (equally weighted) of the brightest clusters defined in scale-free fashion: the most massive clusters (within a radius of $1.0h^{-1}$Mpc comoving) which contain 20% of total mass in the universe at each epoch. The open circles are the results from the 512^3 cell simulation and the solid dots are from the 256^3 cell simulation with 2σ *statistical* errorbars. The solid lines are the best Kaiser fits for the power law model in question: $T(z) = T_0(1+z)^{-1}$. It is seen that the results agree with analytical predictions very well.

Fig. 2.— shows r_{100} as a function of redshift. Here, r_{100} is the average radius of top 20% (in mass) clusters at each redshift with which the average density of each cluster is $100\bar{\rho}(z)$ [$\bar{\rho}(z)$ is the global mean at z].

Fig. 3.— shows the redshift dependence of the core radius (equally weighted) of the same brightest clusters as shown in Figure 1 (defined in scale-free fashion). The open circles are the results from the 512^3 cell simulation and the solid dots are from the 256^3 cell simulation with 2σ *statistical* errorbars. The solid curves are the best Kaiser fits for the power law model in question in the form, $r_{core}(z) = r_0(1+z)^{-2}$.

Fig. 4.— shows derived $\alpha(z)$ (solid squares) and $r_{true}(z)$ (open circles) as a function of redshift in the range $z = 0 - 1$. Here r_{true} is the core corrected radius.

Fig. 5.— shows the linear r.m.s. density fluctuations as a function of top-hat comoving radius for the actual smoothed, truncated power law spectrum (solid curve), which is used in the simulations. Also shown as the dashed curve is that for an ideal, untruncated k^{-1} power law spectrum without the small scale power truncation.

Fig. 6.— The open circles and solid curve represent a fit to the profile averaged over all simulations (but dominated by the few highest resolution simulations) presented in Frenk et al. (1998). The dashed curve is the smoothed profile of the solid curve by a gaussian

with $\sigma_r = \alpha \Delta l$ with $\alpha = 1.65$. We see the result computed in the core regions by our code does in fact correspond well to a gaussian smoothed version of the true density profile if the smoothing length is taken to be 1.65 cells.

Fig. 7.— shows the computed core radii, the corrected core radii, the computed number of X-ray clusters brighter than $L > 10^{43}$ erg/sec, and corrected number of X-ray clusters brighter than $L > 10^{43}$ erg/sec, in the SCDM model, from redshift zero to one. The errorbars are 1σ *statistical*.

Fig. 8.— shows the computed core radii, the corrected core radii, the computed number of X-ray clusters brighter than $L > 10^{43}$ erg/sec, and corrected number of X-ray clusters brighter than $L > 10^{43}$ erg/sec, in the ΛCDM model, from redshift zero to one. The errorbars are 1σ *statistical*.

Figure 1

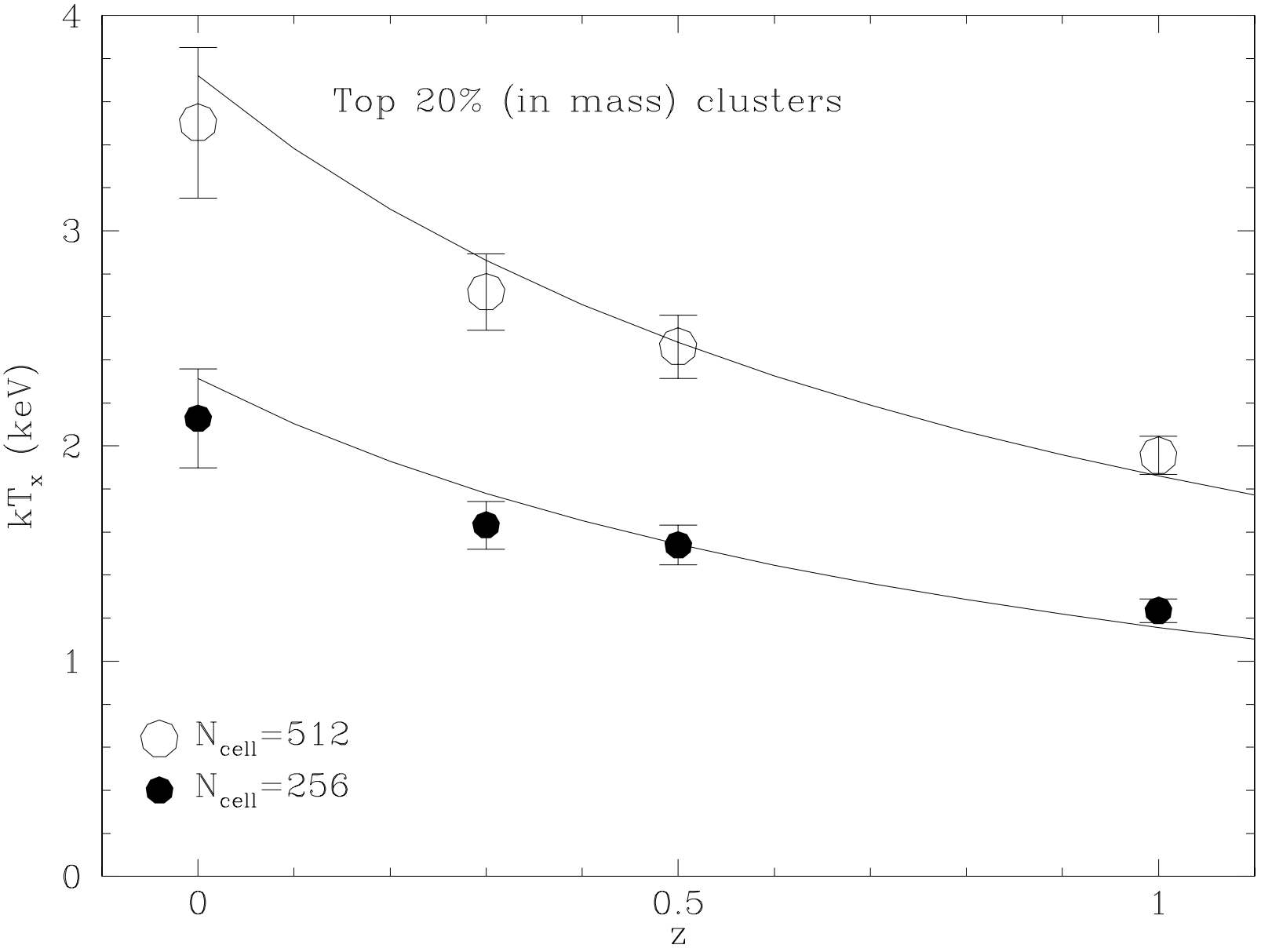
Top 20% (in mass) clusters
N_{cell}=512
N_{cell}=256
kT_x (keV)
z
0
1
2
3
4
0
0.5
1

Figure 2

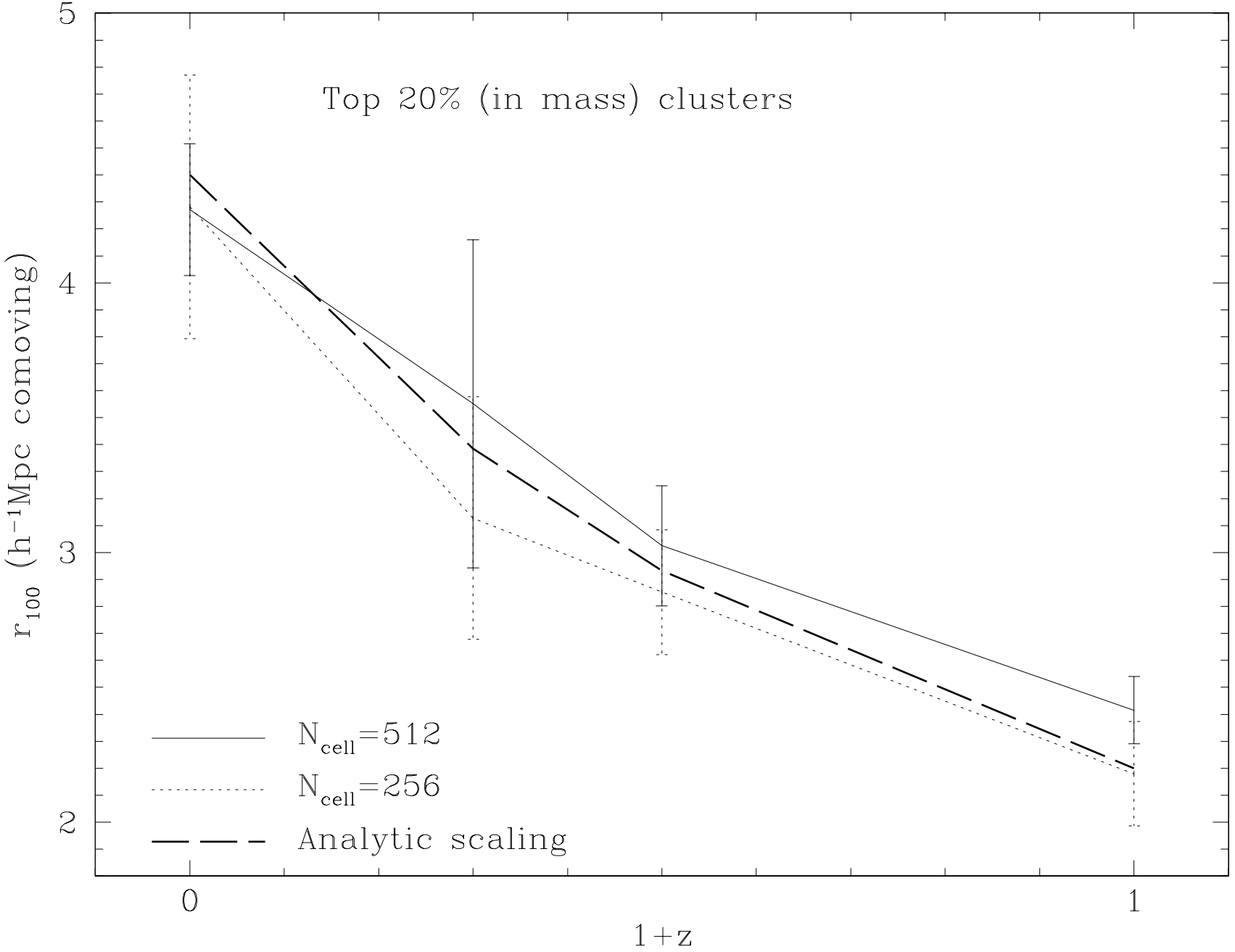
Top 20% (in mass) clusters
r_{100} (h^{-1}Mpc comoving)
5
4
3
2
0
1
1+z
N_{cell}=512
N_{cell}=256
Analytic scaling

Figure 3

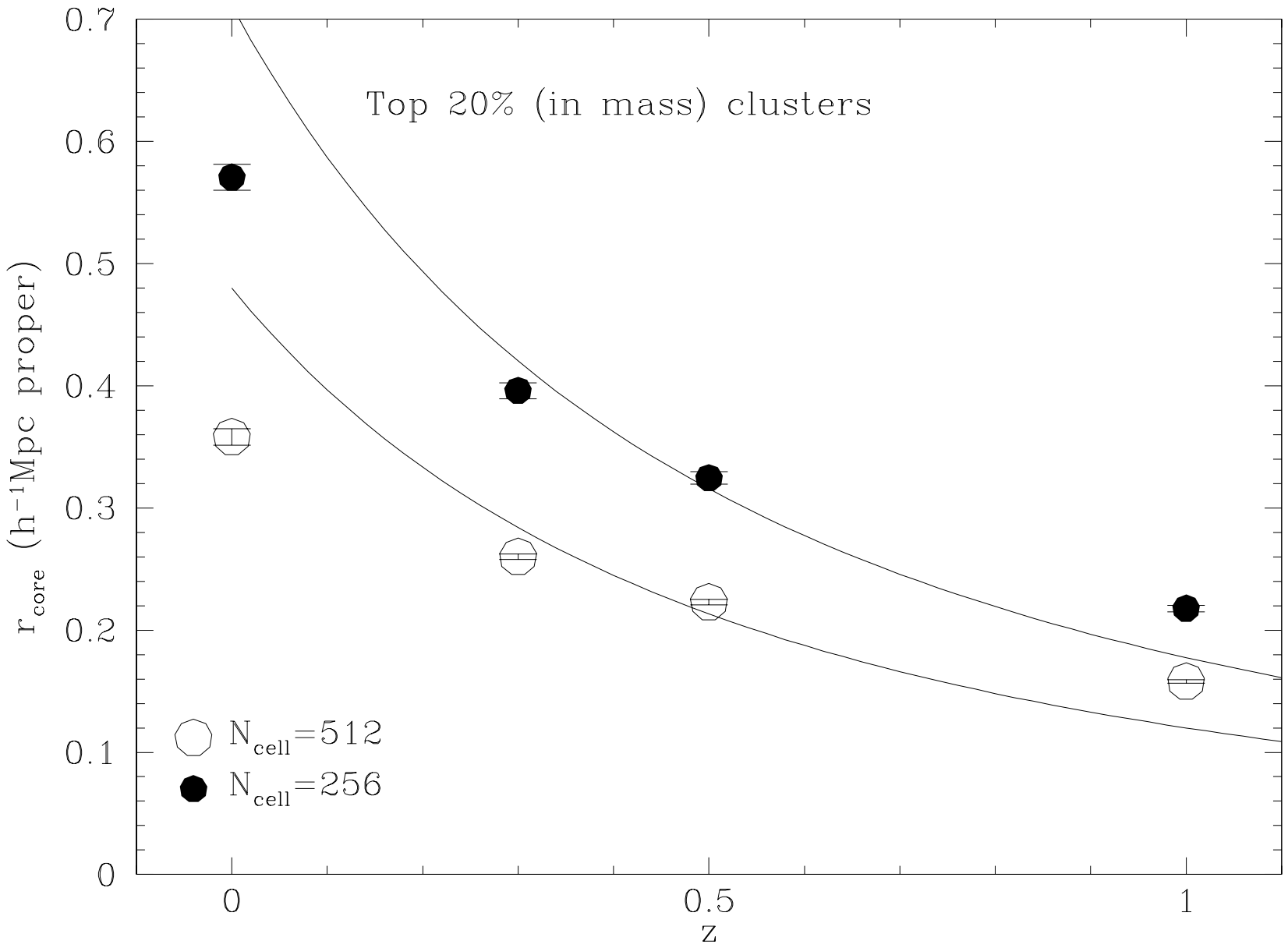
Top 20% (in mass) clusters
r_{core} (h^{-1}Mpc proper)
z
0
0.1
0.2
0.3
0.4
0.5
0.6
0.7
0
0.5
1
N_{cell}=512
N_{cell}=256

Figure 4

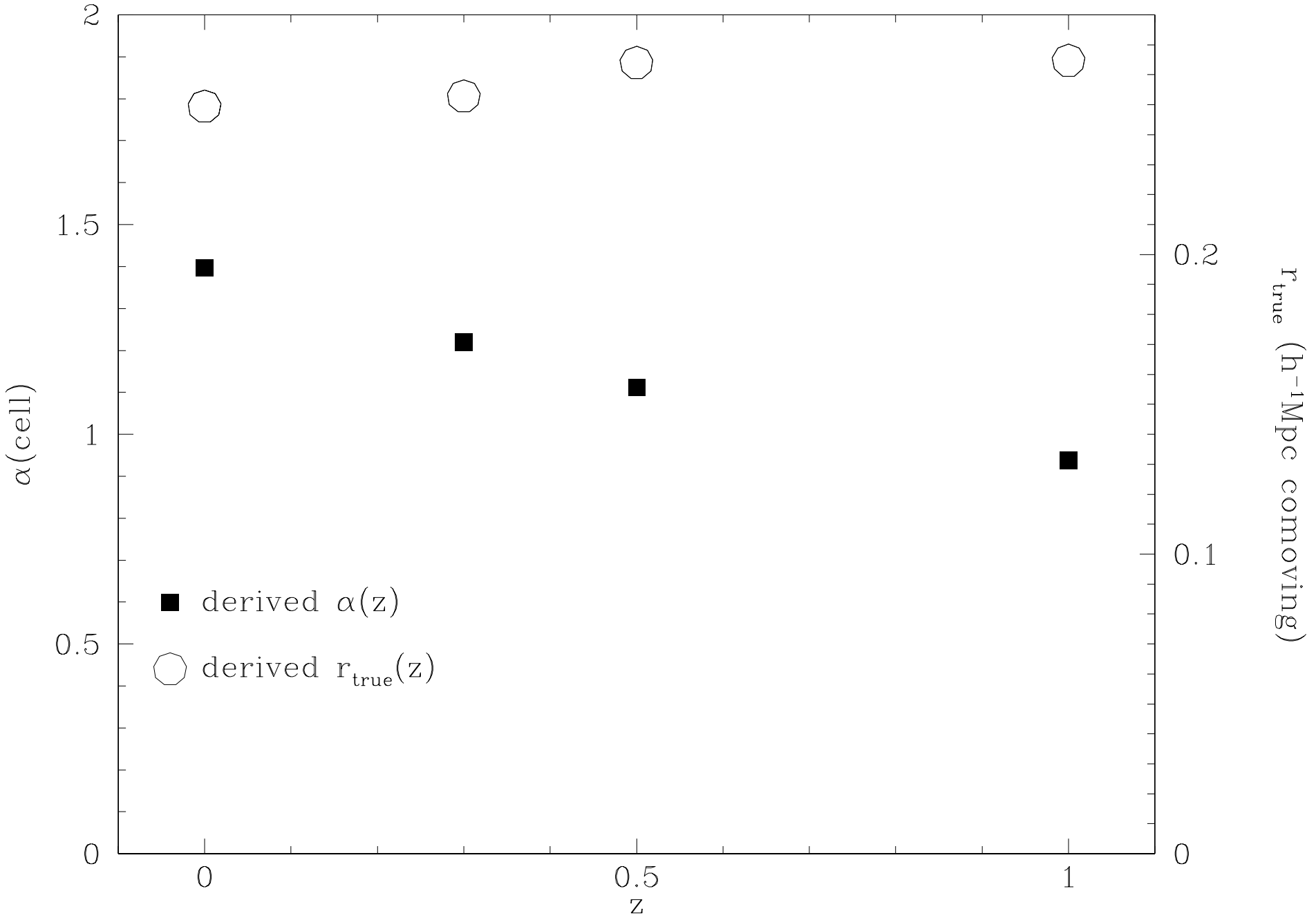
2
1.5
1
0.5
0
0
0.5
1
z
α(cell)
0.2
0.1
0
r_true (h^-1Mpc comoving)
derived α(z)
derived r_true(z)

Figure 5

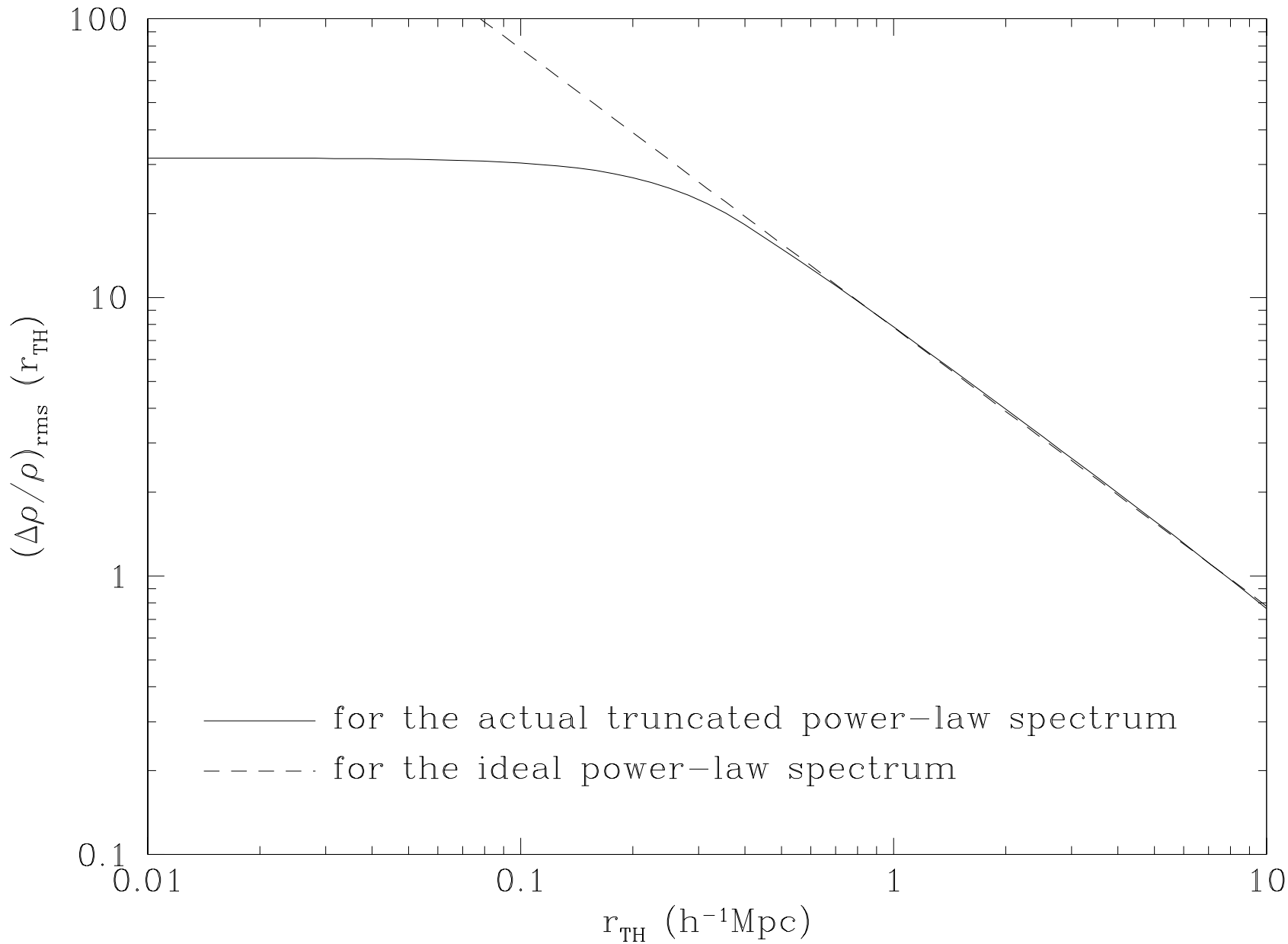
100
10
1
0.1
0.01
0.1
1
10
$(\Delta\rho/\rho)_{rms}$ (r_{TH})
r_{TH} $(h^{-1}Mpc)$
for the actual truncated power−law spectrum
for the ideal power−law spectrum

Figure 6

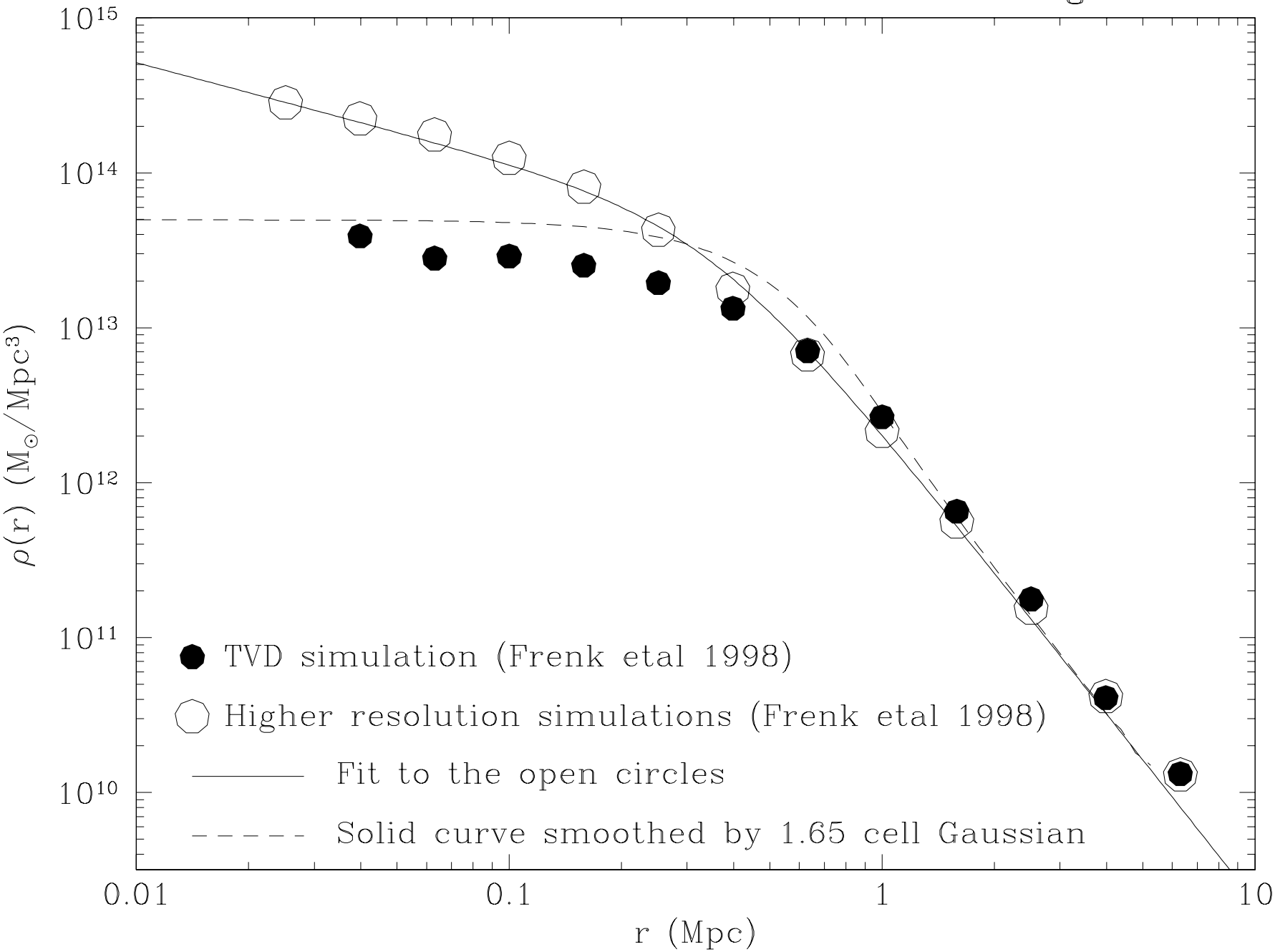
10^{15}
10^{14}
10^{13}
10^{12}
10^{11}
10^{10}
$\rho(r)$ ($M_\odot$/Mpc^3)
0.01
0.1
1
10
r (Mpc)
TVD simulation (Frenk etal 1998)
Higher resolution simulations (Frenk etal 1998)
Fit to the open circles
Solid curve smoothed by 1.65 cell Gaussian

Figure 7

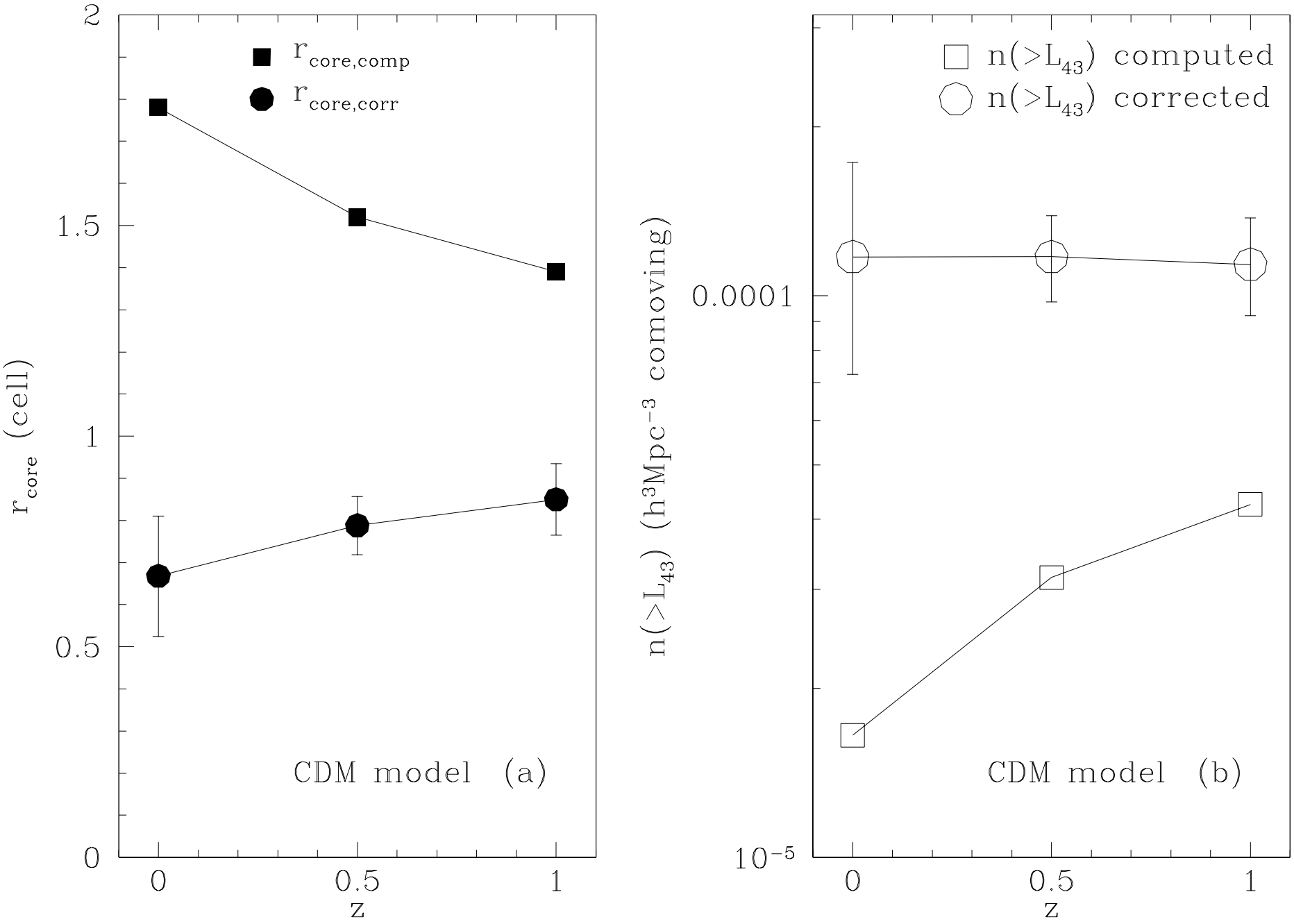
r_core,comp
r_core,corr
r_core (cell)
CDM model (a)
z
n(>L_43) computed
n(>L_43) corrected
n(>L_43) (h^3Mpc^-3 comoving)
CDM model (b)
z

Figure 8

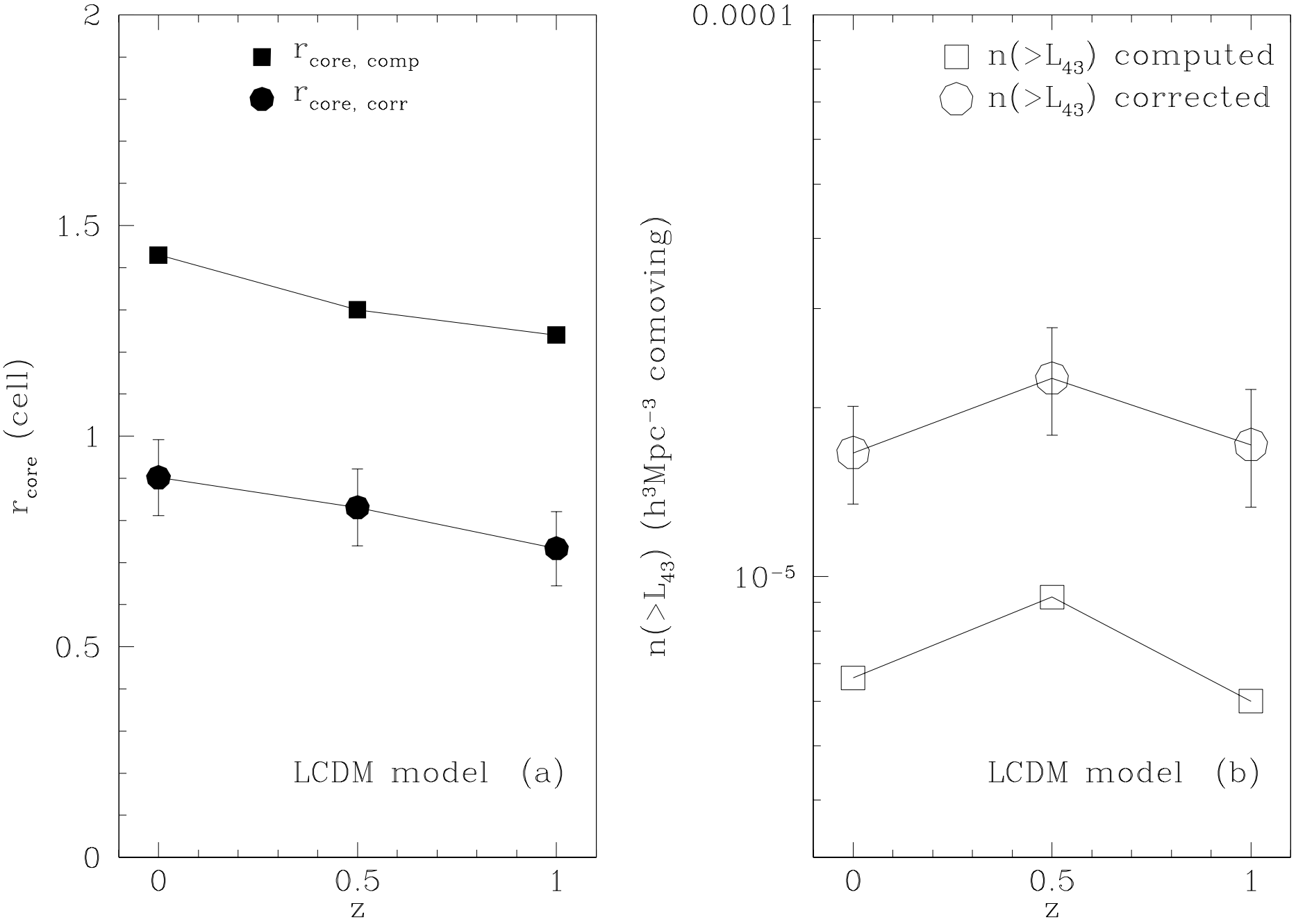
$r_{core, comp}$
$r_{core, corr}$
r_{core} (cell)
z
LCDM model (a)
$n(>L_{43})$ computed
$n(>L_{43})$ corrected
$n(>L_{43})$ (h^3Mpc^{-3} comoving)
LCDM model (b)